Effect of electric field on excitons in a quantum well under additional optical excitation

© *M.A. Chukeev*[1], *E.S. Khramtsov*[1], *Shiming Zheng*[1], *I.V. Ignatiev*[1], *S.A. Eliseev*[2], *Yu.P. Efimov*[2]

[1] Spin Optics Laboratory, Saint Petersburg State University,
198504 St. Petersburg, Russia
[2] Resource Center „Nanophotonics", St. Petersburg State University,
198504 St. Petersburg, Russia

E-mail: maxchukeev@gmail.com

Reflection spectra of a heterostructure with a GaAs/AlGaAs quantum well (QW) of 30 nm wide have been studied under additional optical excitation in an external electric field. The influence of the electric field on all parameters of light-hole and heavy-hole exciton resonances, was studied upon selective excitation of various optical transitions. The effect of compensating for the Stark shift upon excitation to the ground exciton state of the QW is found. A sharp increase in the Stark shift of excitons in QW was found upon optical creation of charge carriers in the GaAs buffer layer. A microscopic calculation of exciton states in various electric fields has been performed. A comparison of the calculated and measured Stark shift of the heavy-hole exciton is used to obtain the dependence of the electric field strength in the QW on the applied voltage.

Keywords: exciton, electric field, quantum well, reflection spectra.

1. Introduction

Optical methods of information processing are considered as a promising way for further development of computing systems. Materials with high optical nonlinearity are needed to implement such methods. These include semiconductor nanostructures with exciton resonances, the optical susceptibility of which can be controlled using an external electric field. In sufficiently wide quantum wells polarized excitons can interact as dipoles, so the electric field allows one to control the interaction of excitons and thereby the resonant optical nonlinearity [1]. On the other hand, the electric field reduces the exciton-light interaction due to a decrease of the overlap of electron and hole wave functions. This can lead to a significant increase in the exciton lifetime, in particular, in coupled quantum wells (QWs), where various nonlinear effects are observed, including Bose condensation of exciton polaritons [2–6]. Thus, it is relevant to search for the optimal range of electric field strengths at which the exciton-exciton interaction has significantly increased, and the exciton-light interaction has not yet been strongly suppressed.

In addition to these effects, the electric field can lead to other effects unrelated to the exciton-exciton interaction. The polarization of the exciton in small fields leads to a decrease in the Coulomb interaction between the electron and the hole in the exciton, which reduces the exciton binding energy [7,8]. An electric field applied along the growth axis of the heterostructure shifts the electron to one potential barrier, and the hole to another. This leads to the formation of the exciton dipole moment and, with the growth of the field, to a shift in the energy of exciton transitions to the red region of the spectrum, the so-called Stark shift of exciton energy [7–10]. Moreover, in sufficiently strong electric fields, the potential barriers for the electron and the hole in the exciton decrease. The electron and the hole can tunnel through these barriers, which leads to exciton ionization. In other words, in addition to radiation recombination, the exciton can decay into free electron and hole, that leads to a reduction in the exciton lifetime in sufficiently strong fields and wide QWs. This is observed in the experiment as an additional homogeneous broadening of exciton transitions [11]. In addition to the above described processes, other effects of the electric field are possible, such as mixing of the states of light and heavy holes [12], the appearance of forbidden transitions [13], suppression of inhomogeneous broadening of exciton states caused by the built-in fluctuating fields [14], localization and Bose condensation of excitons in electrostatic traps [15–17]. Free charges may also be present in the heterostructure, for example, due to background doping of the heterostructure or optical excitation with high photon energy. In this case, the application of an electric field can lead to the movement of free charges, which causes partial or complete screening of the field in the QW under study. The variety of phenomena caused by electric fields greatly complicates the interpretation of the effects observed in the experiment.

Additional optical excitation into various exciton states of QW, as well as the states of the GaAs buffer layer, was used in this paper to study the exciton-exciton interaction in a QW when an electric voltage is applied to the heterostructure. Additional excitation of the buffer layer made it possible to detect an indirect effect of charge carriers generated in it on the behavior of exciton resonances in the QW. Resonant excitation into the ground state of the heavy-hole exciton made it possible to detect the effect of dipole-dipole interaction compensating for the Stark

effect. A strong impact of the electric field on the second quantum confined state of the heavy-hole exciton, which is practically not observed in the absence of the field, was also found. The main results were obtained by experimental investigation of reflection spectra and their modeling, which allows quantitative analysis of all parameters of exciton resonances [18–21]. A microscopic calculation of exciton states in the QW in various electric fields was performed to interpret the effects observed in the electric field.

2.　Experiment technique

The studied sample is a high-quality heterostructure with a 30-nm GaAs/AlGaAs QW grown by molecular beam epitaxy on a *n*-doped GaAs:Si substrate. The structural diagram of the sample is shown in Figure 1.

The barrier layers are short-period AlAs/GaAs superlattices with an average aluminum concentration of 15%. The substrate is separated from the barriers by a GaAs buffer layer with a thickness of 900 nm. The total thickness of all undoped epitaxial layers is 1310 nm. An electric field was applied along the growth axis of the structure. One of the contacts was the doped substrate, and the top contact is the indium and tin oxide (ITO). The electronic band structure is shown in Figure 1. Additional optical pumping was used in various spectral regions, in particular, in the exciton transition of the GaAs buffer layer ($\hbar\omega_1 = 1.516$ eV) and in the ground state of a heavy-hole exciton ($\hbar\omega_2 = 1.521$ eV) to study the exciton-exciton interaction in the QW layer.

The reflection spectra were measured using a low-power continuous-wave light source (a halogen incandescent lamp) at the almost normal light incidence. The short-wave radiation of the lamp was cut off by a broadband optical filter to exclude undesirable excitation of states above the spectral region under study. As an additional source of excitation, the radiation of a tunable titanium-sapphire laser focused into a spot with a diameter of 120 μm was used. The sample was cooled in a closed-cycle cryostat to a temperature of 10 K. The spectra were recorded using a spectrometer with a diffraction grating of 1200 gr/mm and a focal length of 550 mm, equipped with a matrix photodetector (CCD) cooled with liquid nitrogen.

3.　Experimental results

Figure 2 shows the reflection spectra of the investigated heterostructure with additional optical excitation below the exciton resonances of the QW, measured at several values of the applied voltage.

The experiment showed that, in the absence of voltage, the reflection spectrum is insensitive to weak optical excitation ($P = 30\,\mu$W). Three exciton resonances are observed, which corresponds to the ground quantum confined states of the heavy-hole ($Xhh1$) and light-hole ($Xlh1$) exciton and the second quantum confined state of the heavy-hole exciton ($Xhh2$). The shape of the reflection contours of exciton
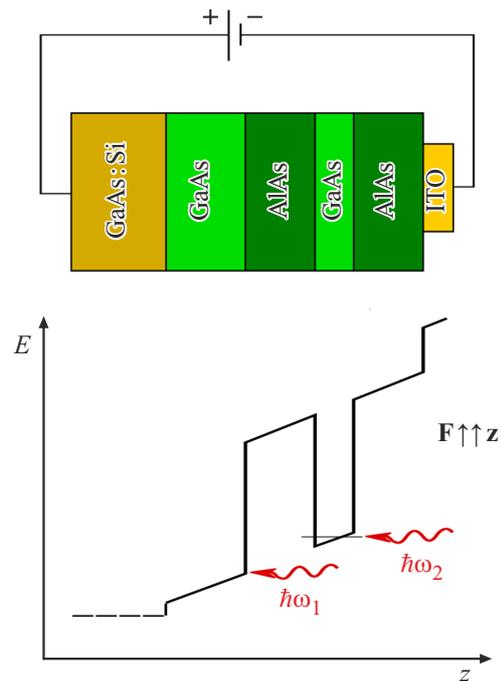
Figure 1. The block diagram of the studied sample (above) and the electronic band structure (below) when a negative potential is applied to the surface of the sample.
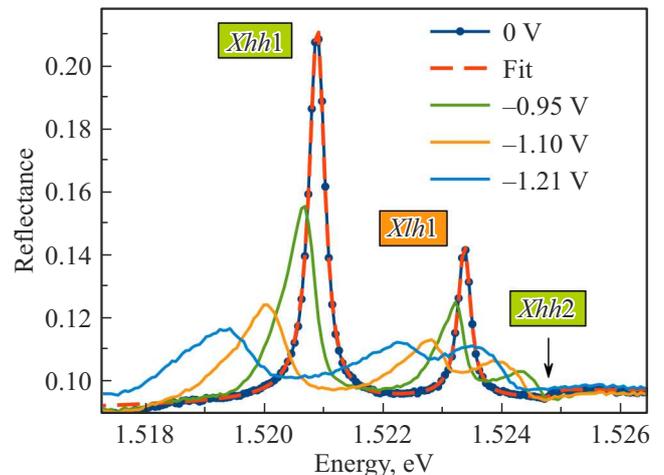
Figure 2. Exciton reflection spectra with additional excitation below exciton resonances of QW with pumping power $P = 30\,\mu$W and various electrical voltages. Exciton resonance energies in the absence of voltage: $E_{Xhh1} = 1.5209$ eV, $E_{X1h1} = 1.5233$ eV, $E_{Xhh2} = 1.5248$ eV. The dashed red curve shows the fitting of the reflection spectra within the framework of the dielectric response model [21]. (A color version of the figure is provided in the online version of the paper).

resonances is due to the interference of light reflected from the sample surface and from the QW layer. It depends on the phase difference between these light waves, which is determined by the distance between the QW layer and the sample surface [18,22]. The thicknesses of the epitaxial

layers were chosen in such a way that the resonances of the ground exciton states appear in the reflection spectra in the form of peaks.

The application of an electric field leads to a broadening of the resonances and their shift towards lower energies. In addition, an increase in voltage leads to the appearance of a resonance corresponding to the excited exciton state $Xhh2$, as well as to the broadening and shift of this resonance to the low energy region with a noticeable phase change. The reflection spectra were studied in this paper when a negative potential was applied to the sample surface.

We modeled the reflection spectra for a detailed study of the effect of the electric field on exciton resonances. The reflection spectrum can be described within the framework of the dielectric response model for high-quality structures in which there is no noticeable contribution of inhomogeneous broadening of exciton resonances [21,23]:

$$R(\omega) = \left| \frac{r_s + r_{QW}}{1 + r_s r_{QW}} \right|^2, \quad (1)$$

where $r_{QW} = \sum_j r_j e^{i2\phi_j}$, and

$$r_j = \frac{\Gamma_{0j}}{(\omega_{0j} - \omega) - i(\Gamma_{0j} + \Gamma_j)}. \quad (2)$$

Here $R(\omega)$ is the total reflection coefficient from the heterostructure, r_s is the amplitude reflection coefficient from the sample surface, r_j is the reflection coefficient of a separate exciton resonance, r_{QW} is the reflection coefficient from the QW, taking into account all exciton resonances. The above formulas contain a number of modeling parameters, namely, the spectral position of the resonance ω_{0j}, radiation broadening $\hbar\Gamma_{0j}$, non-radiation broadening $\hbar\Gamma_j$ and the phase of the light wave ϕ_j. They are used as free fitting parameters and are determined from the experiment.

The red dotted line in Figure 2 shows the result of fitting the reflection spectrum according to the formulas (1) and (2). As it can be seen from the figure, the shape of the main features in the reflection spectra $R(\omega)$ determined by exciton resonances is well described by theoretical formulas, which makes it possible to determine the main parameters of the resonances. In particular, the radiation broadening of exciton resonances $\hbar\Gamma_{0j}$ in the zero field turns out to be equal to $27\,\mu$eV for $Xhh1$ and $10\,\mu$eV for $Xlh1$. The nonradiative broadening of the resonances is of about $100\,\mu$eV. Phase $\phi = 0.06$ rad for $Xhh1$ and $\phi = 0.08$ rad for $Xlh1$. The error of determining the phase is ±0.02.

The obtained results allow us to study the effect of the electric field for all resonances. However, the appearance of the resonance $Xhh2$ and its mixing with the resonance $Xlh1$ in large fields gives rise to a large error in determining the parameters of these resonances. Additional features corresponding to excited quantum confined exciton states are also observed in reflection spectra, in particular, $Xhh3$ and $Xlh2$. These features, as well as the behavior of the resonance $Xhh2$, are not analyzed in this paper. As a

result of modeling the reflection spectra, the dependences of all parameters of exciton resonances in the studied heterostructure on the applied voltage were determined. However, we consider in this paper to discussing only the energy shift of the exciton resonance $Xhh1$.

Figure 3 shows the energy shifts of the exciton resonance $Xhh1$ when the sample is excited to different spectral points. It can be seen that, in the absence of the excitation, the position of the resonance practically does not depend on the voltage. Additional optical excitation leads to a shift of the exciton resonance at a voltage of $|U| > 0.7$ V.

In the case of weak excitation ($P = 30\,\mu$W, see Figure 3, a), the shift magnitude depends on the spectral region of the excitation. In particular, the excitation in to the $Xhh1$ or $Xlh1$ state causes to much smaller shifts than in the case of the excitation in to the buffer GaAs layer. Moreover, the shift practically does not change at the voltage $|U| > 1.1$ V and it is equal to $\Delta E = -0.65$ meV for the excitation to resonance $Xhh1$ and $\Delta E = -0.44$ meV for the excitation to resonance $Xlh1$.

Excitation into the spectral region of the buffer layer causes a significantly larger shift of the exciton resonance $Xhh1$, and at a voltage $|U| = 1.15$ V it is equal to $\Delta E = -1.2$ meV. An increase in the laser pumping power ($P = 160\,\mu$W) leads to a qualitatively different result (Figure 3, b). Namely, the resonance shift with additional excitation into exciton resonances and into the buffer layer causes the same effect. The obtained dependencies for $U < -0.7$ B $= U_{QW}$ are well adjusted by the phenomenological formula:

$$\Delta E = a(U - U_{QW})^b, \quad (3)$$

The fit gives the following parameter values: $a = -7$ meV$\cdot$V^{-b} and $b = 2.2$ for $P = 30\,\mu$W; $a = -14$ meV$\cdot$V^{-b} and $b = 2.2$ for $P = 160\,\mu$W.

4. Discussion of results

4.1. Stark effect

First of all, we will discuss the shift of exciton resonance due to the Stark effect. The exciton resonance $Xhh1$ practically does not shift without additional optical excitation when a voltage is applied (Figure 3). At the same time, the field strength that can be created by the applied voltage and the potential of the Schottky barrier (U_{Sh}) at the ITO/GaAs heterointerface is quite large. It is defined by the expression

$$F = \frac{U_{Sh} + |U|}{\varepsilon L}. \quad (4)$$

The maximum value of the applied voltage is $|U|_{max} = 1.2$ V for the experimental data presented in Figure 3. The Schottky potential value, $U_{Sh} = 0.6$ V, was determined from the current-voltage characteristic of the sample measured at positive bias on the ITO-electrode. The value of static dielectric constant at low temperatures is taken from [24],
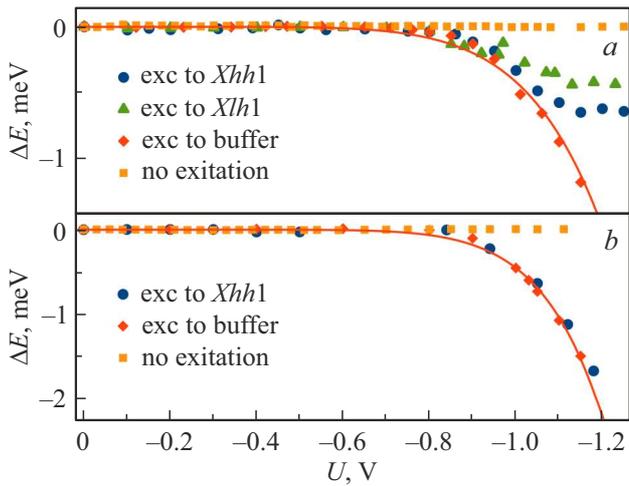
Figure 3. Dependence of the $Xhh1$ exciton resonance energy shift on the magnitude of the applied voltage at the pump power of additional excitation $P = 30 \, \mu\text{W}$ (a), $P = 160 \, \mu\text{W}$ (b). Orange squares show the shift of $Xhh1$ resonance without additional excitation, red diamonds with excitation to the buffer layer, blue dots with excitation to the $Xhh1$ resonance, green triangles with excitation to the $Xlh1$ resonance. The red curves show phenomenological fits by the formula (3). (A color version of the figure is provided in the online version of the paper).

$\varepsilon = 12.53$. The total thickness of the undoped epitaxial layer in the investigated heterostructure is $L = 1.3 \, \mu\text{m}$. The maximum field strength is $F_{\max} = 1.1 \, \text{kV/cm}$ in such conditions. The calculations described in the next section show that, at such a field strength, the exciton resonance should be shifted by the value $\Delta E = -0.1 \, \text{meV}$. This value is greater than the experimental error of the exciton resonance energy ($\delta E \leq 0.01 \, \text{meV}$).

The absence of any noticeable shift in the exciton resonance can be explained by partial screening of the electric field by free charge carriers, which are inevitably present due to background doping of the heterostructure. We can estimate the charge density required for such screening using the model of flat capacitor. The surface density of charge careers required for screening of field $F = 1.1 \, \text{kV/cm}$ is equal to:

$$\sigma = \varepsilon_0 \varepsilon F = 0.12 \, \text{C}/\mu\text{m}^2, \qquad (5)$$

where $\varepsilon_0 = 8.85 \cdot 10^{-14} \, \text{C}/(\text{V} \cdot \text{cm})$. Hence, the bulk density of free charge carriers can be expressed by the formula

$$n_{ch} = \sigma/(q_e L). \qquad (6)$$

As a result, the bulk density of free charge carriers turns out to be $n_{ch} = 60 \, \mu\text{m}^{-3} = 6 \cdot 10^{13} \, \text{cm}^{-3}$. Here $q_e \approx 1.6 \cdot 10^{-19} \, \text{C}$ is the electron charge.

The resulting charge carrier density is small and, in principle, can be provided by background doping. However, the investigated heterostructure has a peculiar feature, due to which the concentration of free carriers in the GaAs

buffer layer is significantly lower than that required to compensate for the electric field. As the photoluminescence spectra show, the grown heterostructure contains an excess of acceptor levels created by carbon impurities. Since the buffer layer is in the contact with the n-doped GaAs substrate, these levels are partially populated with electrons, which reduce the concentration of free hole states. Therefore, we assume that the electric field is not completely screened in the buffer layer. Experiments with optical excitation of the buffer layer confirm this assumption.

The electric field can be screened by background charge carriers in a QW, since it is separated from the substrate by a barrier layer. Moreover, the concentration of free carriers in the QW may be even greater than in the other layers of the heterostructure, since some of the free carriers can be captured in the QW from the barrier layers. Therefore, we assume that the absence of a noticeable energy shift of the exciton state is explained by the compensation of the external electric field by the internal field arising due to the movement of free charge carriers in the QW layer, and not in the entire heterostructure.

Additional optical excitation into the absorption region of the buffer layer leads to a shift of the exciton resonance (Figure 3). Photoexcited charge carriers, unlike the background charge carriers, are very mobile, therefore they are easily separated by the applied voltage in the buffer layer. This leads to two important effects. Firstly, the radiative lifetime increases dramatically, as the overlap of the wave functions of electrons and holes decreases. Secondly, in the extreme case, it is limited only by the nonradiative lifetime of carriers, which in the studied structures is tens of nanoseconds [23,25,26]. This results in the accumulation of photoexcited charge carriers in the buffer layer. We have evaluated their concentration for the case of a relatively weak optical excitation power, $P = 30 \, \mu\text{W}$, and a surface area of $S \approx 10^{-4} \, \text{cm}^2$, with the energy of exciting photons, $E_{\text{phot}} = 2.4 \cdot 10^{-19} \, \text{J}$, using the formula

$$n_{\text{buf}} = \frac{P \tau \alpha}{E_{\text{phot}} S d} = 80 \, \mu\text{m}^{-3}. \qquad (7)$$

Here $\alpha = (1 - R_{\text{ITO}})(1 - e^{-kd})$ is the light absorption coefficient in the buffer layer. Here, we took into account the partial reflection of the exciting light from the surface of the ITO electrode ($R_{\text{ITO}} = 0.09$) and the absorption index, $k = 1.1 \cdot 10^4 \, \text{cm}^{-1}$, on the wavelength of optical excitation [27]. We also assumed that in the case of an external electric field, the lifetime of electron-hole pairs is limited by their nonradiative time, $\tau = 10^{-8} \, \text{s}$. The resulting value of the density of photoexcited charge carriers given by equation (7) exceeds the required value (see equation (6)), so the electric field in the buffer layer can be completely screened.

In this case, the voltage is applied to the epitaxial layer, which includes only the barriers and the QW, with the total thickness of $L_{\text{eff}} = 0.41 \, \mu\text{m}$. The field strength increases strongly, which causes a significant shift in the exciton resonance. This is the second important effect of additional

excitation to the buffer layer. Experiments show that the used pumping power $P = 30\,\mu$W is close to the minimum value at which this effect is observed. With the increase of pumping power, the magnitude of the $Xhh1$ exciton shift increases slightly, however its behavior remains similar (Figure 3).

4.2. Compensation for the Stark effect

Selective excitation into exciton resonances causes the compensation for the Stark shift of excitons. One of the mechanisms explaining this behavior of exciton resonances may be the dipole-dipole interaction of polarized excitons [4] at a sufficiently high two-dimensional density in QW. Such interaction should lead to the repulsion of excitons and, accordingly, to the blue shift of exciton resonances. Moreover, the laser excitation into resonance $Xhh1$ results in the accumulation of excitons in the QW, namely, in a non-radiative exciton reservoir due to their long lifetime [25]. Their interaction with bright excitons should lead to the increase of the repulsion of excitons and, accordingly, the increase of the blue shift of exciton resonances. Thus, the partial compensation for the Stark shift observed in Figure 3, a for $|U| > 1.1\,$V can be caused by the dipole-dipole repulsion of excitons.

We can make a simple estimate of the exciton concentration in the QW and the energy of their dipole-dipole interaction to verify this assumption. A formula similar to formula (7) is used to estimate the two-dimensional exciton density:

$$n_{\text{QW}} = \frac{P\tau\alpha_X}{E_{\text{phot}}S}. \quad (8)$$

Assuming that the exciton lifetime in a non-emitting reservoir $\tau = 30\,$ns and the light absorption coefficient at the exciton resonance, $\alpha_X = 2\Gamma_0/\Gamma = 0.2$, we obtain for the excitation power $P = 30\,\mu$W the following value of two-dimensional density: $n_{\text{QW}} = 75\,\mu$m^{-2}. This corresponds to the average distance between excitons, $a_{dd} = 1/\sqrt{n_{\text{QW}}} = 0.12\,\mu$m.

We have calculated the dipole moment of the $Xhh1$ exciton at the field strength $F = 4\,$kV/cm to estimate the energy of the dipole-dipole interaction of excitons, using the results of microscopic calculation of exciton states. It turned out that, at such a field strength, the static dipole moment of the exciton $P_X = q_e d \approx 10^{-21}\,C\cdot\mu$m. Here $d \approx 6\,$nm is the average distance between an electron and a hole in an exciton in such an electric field.

For a rough estimate of the interaction, let us consider a square lattice of excitons in a QW layer with a lattice constant a_{dd}. The dipole-dipole interaction of one exciton with the other excitons in the lattice is described by the formula

$$E_{dd} = s\,\frac{P_X^2}{4\pi\varepsilon_0\varepsilon a_{dd}^3}. \quad (9)$$

Here the multiplier $s \approx 9$ is obtained by summing over the lattice. We obtain the following estimate for the exciton repulsion energy from this formula: $E_{dd} \approx 0.05\,$meV. The

experimentally observed value of the Stark shift compensation is an order of magnitude greater (Figure 3, a). Thus, dipole-dipole repulsion is not enough to describe the observed compensation effect, and we must look for other mechanisms of this effect.

A possible mechanism for compensating the Stark shift of an exciton may be its ionization in an electric field. Such a process is actively discussed in the literature (see, for example, the article [28] and the references therein). As a result of ionization, free charge carriers are formed, which can partially screen the external electric field. Quantification of the exciton ionization rate in a QW requires separate theoretical modeling, which is beyond the scope of this work.

As the pumping power increases, the compensation of the Stark shift due to the dipole-dipole repulsion of excitons becomes unobservable (see Figure 3, b). This behavior can be explained by the following effects. On the one hand, the light absorption coefficient at the $Xhh1$ transition decreases with an increase in the pumping power due to the broadening of the resonance. As a result, the concentration of excitons generated in the QW, as a function of the pumping power, increases according to the square root law [29]. At the same time, intense laser radiation generates a lot of free charge carriers in the buffer layer, effectively screening the electric field in this layer. Consequently there is a strong increase of the electric field strength in the QW. As a result, the concentration of photogenerated excitons turns out to be insufficient to compensate for the Stark effect.

5. Comparison with theoretical calculation

Exciton can serve as a sensitive probe of various characteristics of the heterostructure as it was shown in [22], in particular exciton located in a QW can give information about the profile of the potential well [30]. Here we use the Stark shift of the exciton as a probe to estimate the electric field strength in the QW. For this purpose, we performed a microscopic calculation of the exciton energy in an electric field. The calculation is model-accurate and does not contain fitting parameters. The values of the material parameters of the heterostructure used in the calculation are well tested in other studies [22,30–33].

The three-dimensional Schrodinger equation [33] was solved numerically for the theoretical description of the exciton in QW in an external electric field:

$$\left(-\frac{\hbar^2}{2\mu_{hxy}}\left(\frac{\partial^2}{\partial\rho^2} - \frac{1}{\rho}\frac{\partial}{\partial\rho} + \frac{1}{\rho^2} \right) - \frac{\hbar^2}{2m_e}\frac{\partial^2}{\partial z_e^2} \right.$$
$$\left. -\frac{\hbar^2}{2m_{hz}}\frac{\partial^2}{\partial z_h^2} + V \right)\chi(\rho, z_e, z_h) = E_x\chi(\rho, z_e, z_h), \quad (10)$$

where

$$V = V_e(z_e) + V_h(z_h) + eF(z_e - z_h)$$
$$-\frac{e^2}{4\pi\varepsilon_0\varepsilon\sqrt{\rho^2 + (z_e - z_h)^2}}. \quad (11)$$

The first term of the Hamiltonian (10) is the kinetic energy operator of the relative motion of an electron and a hole in an exciton in the QW plane (along the coordinates x and y), where ρ is the distance between the electron and the hole, and $\mu_{hxy} = m_e m_{hxy}/(m_e + m_{hxy})$ is reduced exciton mass. The second and third terms are operators of the kinetic energy of the electron and hole motion across the QW, where m_e is the effective mass of the electron, m_{hz} is the effective mass of the hole along the axis z. The calculation takes into account that the mass of the hole is anisotropic, $m_{hz} \neq m_{hxy}$, and it is described using the Luttinger parameters [33]. The last term of the Hamiltonian is the potential energy described by the expression (11). The rectangular potential of QW is described by the terms V_e and V_h for electrons and holes, respectively. The following term describes the influence of an external electric field, where e is the elementary charge of the electron, z_e and z_h are the coordinates of the electron and the hole along the axis z, respectively. The last term describes the energy of the Coulomb interaction between an electron and a hole, where ε is the dielectric constant of the medium. Function $\chi(\rho, z_e, z_h) = \rho\psi(\rho, z_e, z_h)$, where $\psi(\rho, z_e, z_h)$ is exciton wave function. The multiplier ρ was introduced to implement zero boundary conditions at the same coordinates of the electron and the hole.

The numerical implementation is based on the finite difference method, in which the Schrodinger equation is represented in the matrix form [33]. The lowest eigenvalues and eigenvectors of the matrix were computed to determine the exciton energy and the wave function. The error of approximation of the differential equation by finite differences decreases with a decrease in the size of the grid used. The calculation areas for the coordinates ρ, z_e and z_h were 200 nm. The grid size was successively reduced from 2 to ~ 0.9 nm, and then the result was extrapolated to the grid step equal to zero.

The results of calculation of the $Xhh1$ exciton energy shift for several values of the electric field strength are shown in Figure 4. The obtained dependence is approximated using the phenomenological formula:

$$\Delta E = \alpha F^{\beta}. \qquad (12)$$

As a result of the approximation the following parameter values are obtained: $\alpha = -73\,\mu\text{eV} \cdot (\text{kV/cm})^{-\beta}$, $\beta = -2$.

Comparison of the experimentally measured $Xhh1$ resonance shift depending on the applied voltage U with the calculated shift depending on the field strength F makes it possible to estimate the field strength in the experiment. The $F(U)$ dependence obtained for weak ($P = 30\,\mu\text{W}$) and strong ($P = 160\,\mu\text{W}$) optical excitation is shown in the insert of Figure 4.

It can be seen that the field strength in QW is small for the voltage of $|U| < |U_0| \sim 0.7$ V and practically does not depend on the applied voltage. As described above, this may be due to the compensation of the external electric field by free background charge carriers in the layers of barriers and QW. There is no compensation in the region $|U| > 0.7$.
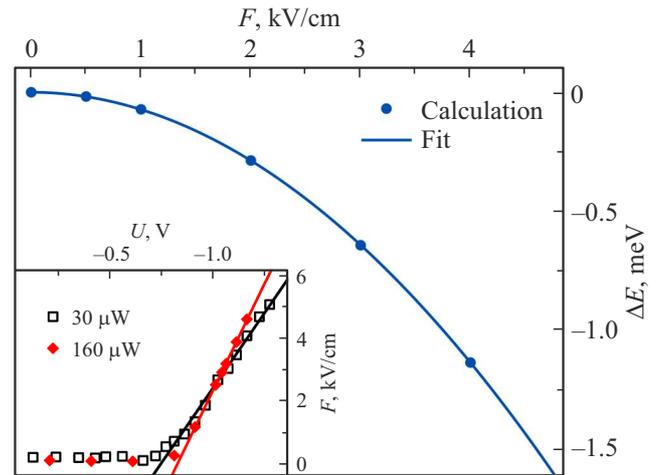
Figure 4. Dependence of the exciton $Xhh1$ resonance shift on the electric field strength obtained in microscopic calculation. The blue curve shows the phenomenological fit with the formula (12). The inset shows the dependence of the electric field strength in the QW layer on the applied voltage at weak ($P = 30\,\mu\text{W}$, hollow squares) and stronger ($P = 160\,\mu\text{W}$, red diamonds) optical excitation into the buffer layer. The black and red straight lines show the fit with the formula $F = k(U - U_0)$ for weak and strong excitations, respectively. (A color version of the figure is provided in the online version of the paper).

This is due to the fact that the carriers are already localized near the potential walls of the QW and they can not compensate the electric field further. Therefore the field strength increases with the increase of the applied voltage. According to formula (4), the obtained dependence of the field strength in the QW on voltage allows us to estimate the thickness of the effective layer L_{eff} to which the voltage is applied.

The following estimate for the effective thickness is obtained from the data given in the insert of Figure 4 for the case of weak excitation into the buffer layer ($P = 30\,\mu\text{W}$): $L_{\text{eff}} \approx 320$ nm. The resulting estimate of L is slightly less than the total thickness of the barriers and the QW, $L_{\text{eff}} = 410$ nm. A possible reason for this may be the partial compensation of the electric field in the barrier layers due to their uncontrolled background doping.

6. Conclusion

We have conducted an experimental study of excitons in the GaAs/AlGaAs QW in an electric field. The analysis of the reflection spectra in the framework of the dielectric response model shows that the application of the electric field to the investigated heterostructure with the QW leads to a significant shift of exciton resonances only in the presence of additional laser excitation. The shift of the $Xhh1$ resonance in the case of excitation into the GaAs buffer layer is well described by the phenomenological formula (3) with the values of the parameters given below this formula. Such a shift of the exciton resonance is due to the Stark effect, which is confirmed by microscopic calculation without use

of fitting parameters. Additional excitation in to the states $Xhh1$ and $Xlh1$ made it possible to detect compensation for the Stark shift of exciton resonances. The theoretical calculation of the exciton level energy made it possible to determine the magnitude of the electric field strength in the QW layer and to estimate the magnitude of the effective layer of the heterostructure to which the voltage is applied.

Funding

Acknowledgments

Conflict of interest

The authors declare that they have no conflict of interest.

References

[1] S.I. Tsintzos, A. Tzimis, G. Stavrinidis, A. Trifonov, Z. Hatzopoulos, J.J. Baumberg, H. Ohadi, P.G. Savvidis. Phys. Rev. Lett., **121** (3), 037401 (2018).

[2] L.V. Butov, A.C. Gossard, D.S. Chemla. Nature, **418**, 751 (2002).

[3] L.V. Butov, C.W. Lai, A.L. Ivanov, A.C. Gossard, D.S. Chemla. Nature, **417**, 47 (2002).

[4] Z. Vörös, D.W. Snoke, L. Pfeiffer, K. West. Phys. Rev. Lett., **103** (1), 016403 (2009).

[5] P. Andreakou, S. Cronenberger, D. Scalbert, A. Nalitov, N.A. Gippius, A.V. Kavokin, M. Nawrocki, J.R. Leonard, L.V. Butov, K.L. Campman, A.C. Gossard, M. Vladimirova. Phys. Rev. B, **91** (12), 125437 (2015).

[6] D.J. Choksy, Chao Xu, M.M. Fogler, L.V. Butov, J. Norman, A.C. Gossard. Phys. Rev. B, **103** (4), 045126 (2021).

[7] D.A.B. Miller, D.S. Chemla, T.C. Damen, A.C. Gossard, W. Wiegmann, T.H. Wood, C.A. Burrus. Phys. Rev. Lett., **53** (22), 2173 (1984).

[8] A. Thilagam. Appl. Phys. A, **64** (1), 83 (1997).

[9] J.A. Brum, G. Bastard. Phys. Rev. B, **31** (6), 3893 (1985).

[10] D.A.B. Miller, D.S. Chemla, T.C. Damen, A.C. Gossard, W. Wiegmann, T.H. Wood, C. Burrus. Phys. Rev. B, **32** (2), 1043 (1985).

[11] L. Schultheis, K. Köhler, C.W. Tu. Phys. Rev. B, **36** (12), 6609 (1987).

[12] R.T. Collins, L. Viña, W.I. Wang, L.L. Chang, L. Esaki, K.v. Klitzing, K. Ploog. Phys. Rev. B, **36** (3), 1531 (1987).

[13] M. Whitehead, G. Parry, K. Woodbridge, P.J. Dobson, G. Duggan. Appl. Phys. Lett., **52** (5), 345 (1988).

[14] I.V. Ponomarev, L.I. Deych, A.A. Lisyansky. Phys. Rev. B, **72** (11), 115304 (2005).

[15] A.V. Gorbunov, V.B. Timofeev. Jetp Lett. **84** (2006). [Pisma ZHETF, **84** (6), 390 (2006). (in Russian).]

[16] A.V. Gorbunov, V.B. Timofeev. Jetp Lett. **96** (2012). [Pisma ZHETF, **96** (2), 145 (2012). (in Russian).]

[17] S.V. Lobanov, N.A. Gippius, L.V. Butov. Phys. Rev. B, **94** (24), 245401 (2016).

[18] E. Ivchenko, P. Kopyev, V. Kochereshko, I. Uraltsev, D. Yakovlev, S. Ivanov, B. Meltzer, M. Kalitievsky. FTP, **22**, 784 (1988). (in Russian).

[19] E. Ivchenko, A. Kavokin, V. Kochereshko, P. Kop'ev, N. Ledentsov. Superlatt. Microstr., **12** (3), 317 (1992).

[20] E. Ivchenko, V. Kochereshko, A. Platonov, D. Yakovlev, A. Baar, B. Occay, G. Landver. FTT **39**, 2072 (1992). (in Russian).

[21] E.L. Ivchenko. *Optical Spectroscopy of Semiconductor Nanostructures* (Springer, Berlin, 2004) p. 437.

[22] P.Yu. Shapochkin, S.A. Eliseev, V.A. Lovtcius, Yu.P. Efimov, P.S. Grigoryev, E.S. Khramtsov, I.V. Ignatiev. Phys. Rev. Appl., **12** (3), 034034 (2019).

[23] A.V. Trifonov, S.N. Korotan, A.S. Kurdyubov, I.Ya. Gerlovin, I.V. Ignatiev, Yu.P. Efimov, S.A. Eliseev, V.V. Petrov, Yu.K. Dolgikh, V.V. Ovsyankin, A.V. Kavokin. Phys. Rev. B, **91**, 115307 (2015).

[24] I. Strzalkowski, S. Joshi, C.R. Crowell. Appl. Phys. Lett., **28** (6), 350 (2008).

[25] A.S. Kurdyubov, A.V. Trifonov, I.Ya. Gerlovin, B.F. Gribakin, P.S. Grigoryev, A.V. Mikhailov, I.V. Ignatiev, Yu.P. Efimov, S.A. Eliseev, V.A. Lovtcius, M. Assmann, M. Bayer, A.V. Kavokin. Phys. Rev. B, **104** (3), 035414 (2021).

[26] A.S. Kurdyubov, A.V. Trifonov, A.V. Mikhailov, Yu.P. Efimov, S.A. Eliseev, V.A. Lovtcius, I.V. Ignatiev. Phys. Rev. B, **107**, 075302 (2023).

[27] M.D. Sturge. Phys. Rev., **127**, 768 (1962).

[28] J. Heckötter, M. Freitag, D. Fröhlich, M. Aßmann, M. Bayer, M.A. Semina, M.M. Glazov. Phys. Rev. B, **98**, 035150 (2018).

[29] D.F. Mursalimov, A.V. Mikhailov, A. Kurdyubov, A.V. Trifonov, I.V. Ignatiev. Semiconductors, **56**, 2021 (2022).

[30] P. Grigoryev, A. Kurdyubov, M. Kuznetsova, I. Ignatiev, Yu. Efimov, S. Eliseev, V. Petrov, V. Lovtcius, P. Shapochkin. Superlatt. Microstr., **97**, 452 (2016).

[31] I. Vurgaftman, J.R. Meyer, L.R. Ram-Mohan. J. Appl. Phys., **89** (11), 5815 (2001).

[32] M.N. Bataev, M.A. Chukeev, M.M. Sharipova, P.A. Belov, P.S. Grigoryev, E.S. Khramtsov, I.V. Ignatiev, S.A. Eliseev, V.A. Lovtcius, Yu.P. Efimov. Phys. Rev. B, **106**, 085407 (2022).

[33] E.S. Khramtsov, P.A. Belov, P.S. Grigoryev, I.V. Ignatiev, S.Yu. Verbin, Yu.P. Efimov, S.A. Eliseev, V.A. Lovtcius, V.V. Petrov, S.L. Yakovlev. J. Appl. Phys., **119**, 184301 (2016).

Translated by A.Akhtyamov

Publication of the Symposium proceedings completed.